Manufacturing Rev. **11**, 7 (2024)

https://doi.org/10.1051/mfreview/2024003

Manufacturing Review
Available online at:
https://mfr.edp-open.org

REGULAR ARTICLE OPEN ACCESS

Microstructural and corrosion behaviours of dissimilar friction stir welded aluminium alloys

Benjamin I. Attah[1], RASAQ O. Medupin[2], Tertsegha D. Ipilakyaa[3], Uzoma G Okoro[4], Oyewole Adedipe[4], Gowon Sule[5], Omolayo Michael Ikumapayi[6,9,*], Katsina C. Bala[4], Esther T. Akinlabi[7], Sunday A. Lawal[4,8], and Asipita S. Abdulrahman[4]

[1] Department of Mechanical Engineering, African University of Science and Technology, Abuja, Nigeria
[2] Department of Materials and Metallurgical Engineering, Federal University of Technology, Owerri, Nigeria
[3] Department of Mechanical Engineering, Joseph Sarwuan Tarka University, Makurdi, Nigeria
[4] Department of Mechanical Engineering, Federal University of Technology, Minna, Nigeria
[5] Department of Aerospace Engineering, Air Force Institute of Technology, Kaduna, Nigeria
[6] Department of Mechanical and Mechatronic Engineering, Afe Babalola University, Ado- Ekiti, Nigeria
[7] Department of Mechanical and Construction Engineering, Northumbria University, Newcastle, United Kingdom
[8] Department of Mechanical Engineering, University of Mines and Technology, Tarkwa, Ghana
[9] Department of Mechanical Engineering Science, University of Johannesburg, South Africa

Received: 31 August 2023 / Accepted: 20 January 2024

Abstract. In this study, the friction stir welding (FSW) process was employed to investigate the effect of tool geometry on the corrosion behaviour and microstructure of friction stir welded AA7075-7651 and AA1200-H19 using Central Composite Design. The workpieces were machined and welded, and the interfaces were milled. A 2-level full factorial experimental design was deployed using Response Surface Methodology (RSM). A rotational speed of 1500 rpm, welding speed of 30, 60, and 90 mm/min, and a 2° tilt angle of the tool with a plunge force of 7 kN were utilized. The results show that regardless of the tool geometry, multi-response optimum weldment can be achieved at 60 mm/min welding speed and a tilt angle. The microstructure of the optimal weldments presents an 'onion ring' pattern, indicating proper mixing of the alloys during FSW. Analysis of the corrosion behaviour revealed a decrease in the polarization resistance when the transverse speed increased from 30 to 90 mm/min, as polarization resistance has a direct relationship with corrosion rate. It can be concluded that FSW ensures excellent weldment, as evident in the microstructural evolution of the resulting weldments, and that tool geometry plays a significant role in the corrosion inhibition efficiency of the alloys.

Keywords: Friction stir welding / microstructure properties / aluminium alloy / central composite design / corrosion behaviour

1 Introduction

Improved technology for excellent joining of dissimilar metallic materials is in high demand for 21st-century industrial applications [1]. The superior corrosion susceptibility and conductivity of aluminium (Al) and copper (Cu), for instance, make them important in this enterprise. Nevertheless, the thermal properties of these two materials qualify them as difficult-to-weld metals as far as conventional welding processes are concerned. Common conventional welding methods form hard and brittle intermetallic phases at the interface of the joint [2]. This eventually introduces potential failure sites, which undermine the integrity of the welded joint. However, friction stir welding (FSW) helps to address the associated challenges [3]. This welding process produces high-quality welds at optimized energy consumption in the absence of gas or flux; hence, it is a safer and more eco-friendly process. Leal et al. [4] and Mohan and Wu [5] submitted that this improvement could significantly reduce energy consumption for implementation on a large scale. And Singh et al. [6] highlighted fixed, adjustable, and self-retracting as FSW types based on the pieces making the tools. In addition, the challenges encountered during the welding of non-ferrous metals are grave in fusion, causing cracks and porosity as well as emitting poisonous gases, compared to solid-state welding. However, the FSW process is adjudged appropriate for welding aluminium alloys, especially in high-performance industrial applications.

* e-mail : ikumapayi.omolayo@abuad.edu.ng

Numerous metallic ancillary parts are used in the aerospace industry. Aside from their weight contribution, they are liable for crevice corrosion, according to Caio-Palumbo et al. [7]. Therefore, deploying the FSW technique eliminates additional weight tendency and eliminates the poisonous gases associated with conventional welding techniques as a green and sustainable technology. It is important to acknowledge that the functionality of friction stir welded links is contingent upon the selection of process variables. If these factors are chosen incorrectly, it might result in the formation of defective joints [8]. The work published by Pankaj et al. [9] is ranked among several researchers who have successfully joined dissimilar materials using the FSW process. They welded plates of AA7075-T6 alloy and found an initial decrease in tensile strength as welding speed increased up to 75 mm/min. In a comparable investigation, Fereiduni et al. [10] conducted an examination of the friction stir spot-welding process, including the joining of ferrous and non-ferrous alloys. According to their findings, a limited duration of dwell time has the potential to impede the formation of welded joints of superior quality. Sezhian et al. [11] and Yoo et al. [12] conducted research on the microstructure and mechanical attributes of dissimilar non-ferrous joints, employing rotational and travel speeds as operational factors. The researchers observed that an increase in travel or rotation speed leads to the emergence of irregular border shapes. Similarly, it was observed that the occurrence of faults was attributed to the inadequate duration available for material mixing in the region of high traverse speed.

In a separate study, Lienert et al. [13] conducted an investigation into the viability of employing the friction stir welding (FSW) technique for the purpose of connecting mild steel. Additionally, it was discovered that several process parameters, such as traverse speed and force, have a substantial impact on the quality of the welded joints. In a recent study conducted by Hadi et al. [14], a comprehensive analysis was performed using the ABAQUS software to develop a three-dimensional numerical model. The primary objective of this study was to estimate the maximum temperature and the distribution of plastic strain in friction stir welding (FSW) of AA5754 joints. The results of their study indicated that an increase in rotational speed is associated with a concurrent rise in peak temperature, whereas an increase in traverse speed leads to a decrease in peak temperature. This finding is consistent with the previous study conducted by Bhatt and Pillai [15], in which they utilized finite element analysis software to simulate the friction stir welding (FSW) process and acquire temperature profiles and flow stresses. The impact of variations in tool welding speed on the temperature profile and flow stresses during friction stir welding (FSW) of materials with constant tool rotational speed and equivalent tool geometry has been described.

Optimizing these parameters is necessitated by the need to produce non-defective welded joints. Hence, Jambulingam [16] examined AA7075 and AA3014 joined by FSW, optimizing the process speed, feed rate, and axial force. Speed was found to be the major factor influencing the physical properties of the joints. Similarly, Amit et al. [17] utilized RSM to optimize FSW parameters for AA3003 joints, focusing on the UTS of AA3003 joints. These authors achieved improved mechanical properties of AA3003 during the studies. In their study, Wang et al. [18] examined the impact of welding speed on the microstructure as well as the mechanical characteristics of a robotic friction stir welding (FSW) process. The researchers aimed to identify the optimal parameters for this process and also investigated the heat inputs associated with various parameter mixtures. Additionally, they explored the correlation between grain size in the stirred zone and the welding parameters. They concluded, like earlier researchers, that real-time tool force responds proportionately to an increase in welding speeds in a stable welding stage and also observed that the grains in the nugget zone became refined recrystallization grains from the initial elongated rolling type. Wang et al. [8] therefore concluded that the strain rate and deformation temperature of welded materials determine the overall grain size.

Therefore, this study is significant as it develops a FSW process to examine the effect of tool geometry on the evolving microstructure and corrosion behaviour of friction stir welded dissimilar Al alloys (AA7075-7651 and AA1200-H19) by utilizing CCD for high-performance applications. This, as far as the authors can tell, is a set of parameters scarcely reported in the literature, at least not in recent decades. The results, therefore, will spur on researchers and other stakeholders who might, hitherto, be sceptical or unaware of the reported possibilities.

2 Materials and methods

2.1 Materials

The primary materials utilized in this study consist of AA7075 and AA1200. The specimens were acquired from Bharat Aerospace Alloys, located in Gulalwadi, Mumbai, India, with the postal code 400:004. Additional materials utilized in the experiment encompassed 320-grit silicon carbide (SiC) paper, acetone, and stir-welding equipment obtained from ETA Technology PVT LTD, namely model WS004, originating from India. Some other examples of equipment used in this field include the electrical discharge machine (ED350/200SP; USA), the backing plate and clamping system (ETA Technology PVT LTD; India), and FSW tools (V3 Instruments; India). The workpieces utilized as basis materials for the welding process were machined to the necessary dimensions by the utilization of a band saw, after which they were subjected to the welding procedure. As a result, the interface underwent a milling process that resulted in an arrangement where, when positioned adjacent to each other, the visibility through the interface is obstructed.

2.2 Experimental design

The study's experimental approach was conducted using Minitab 17 software, employing Response Surface Methodology (RSM) through the use of Central Composite Design (CCD). The study utilized both a tapered tool (TT) and a tapered threaded tool (TTT). The Central Composite Design (CCD) was chosen over Box-Behnken's Design (BBD) due to its inclusion of a 2-level full factorial

Table 1. Factor levels of process parameters.

Parameters	Lower axial point (−α)	Lower cubic point (−1)	Centre point (0)	Upper centre point (+1)	Upper axial point (α)
Rotational speed	900	1150	1500	1850	2100
Transverse speed	30	45	60	75	90
Tool tilt angle	1.0	1.5	2.0	2.5	3.0

Table 2. Experimental design matrix.

Runs	Tilt angle (°)	Standard order	Transverse speed (mm/mm)	Rotational speed (rpm)
1	1.5	10	45	1150
2	1.5	1	45	1850
3	1.5	3	75	1150
4	1.5	6	75	1850
5	2.5	19	45	1150
6	2.5	16	45	1850
7	2.5	4	75	1150
8	2.5	15	75	1850
9	2	9	60	900
10	2	2	60	2100
11	2	14	30	1500
12	2	12	90	1500
13	1	5	60	1500
14	3	8	60	1500
15	2	11	60	1500
16	2	13	60	1500
17	2	7	60	1500
18	2	20	60	1500
19	2	17	60	1500
20	2	18	60	1500

design, axial points (α), and center points. Therefore, the experimental setup incorporated variables such as rotational speed, welding speed, and tilt angle of the tool while maintaining a consistent downward plunge force of 7 kN. Tables 1 and 2 display the factor levels and experimental design matrix for the given process, respectively.

2.3 Friction stir welding process

A shoulder-to-pin ratio of 3:1 was adopted for tool design in line with literature [18]. Cuboidal coupons of $120 \times 60 \times 6$ mm dimensions were used. Thereafter, the joints to be welded were milled, taking into account proper lapping, and they were clamped on the FSW machine in a butt configuration. A 2 mm allowance was created for plastic deformation and bonding towards the softer material (AA1200-H19). This was followed by the cleaning of the joints to be welded to remove coatings that could impede the process, and then washed with acetone to take care of grease. The welding was done automatically, following the process of feeding the welding parameters into the friction stir. The welding procedure described in Attah et al. [19] was adopted in this work. The frictional heat generated increased at the welding region as a result of the increment in the rotational tool speed [11]. This heat softened the stirred materials without melting them. The weldment was allowed to cool at the end of the process and then unclamped. Figure 1 shows the schematics of the adopted friction stir butt welding process.

2.4 Performance evaluation of weld joints

The corrosion analysis was conducted with the Metrohm potentiostat/galvanostat (Autolab PGSTAT101) that was connected to NOVA software version 2.1.2 for data analysis and control. The coupons underwent analysis. To ensure the reduction of contaminants, the surface of each specimen was meticulously cleansed in adherence to the methodology outlined by Ikumapayi et al. [20]. A corrosive solution was created by dissolving 35 grams of sodium chloride in 1 L of distilled water at ambient temperature. Electrochemical experiments were independently performed on both the base metals and the friction stir welded samples. The purpose of this study is to

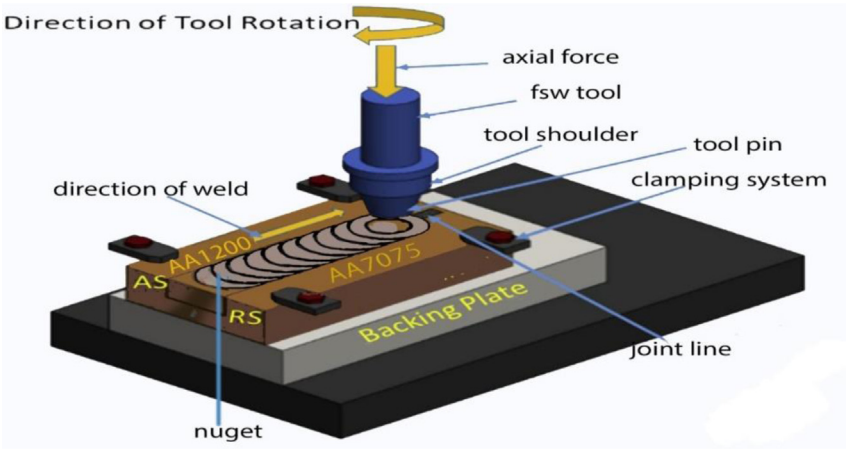

Fig. 1. Process diagram for the two dissimilar aluminium alloys friction stir welded joint [19].

investigate the open circuit potential (OCP) and potentiodynamic polarization (PDP) by utilizing a setup consisting of three electrodes: the reference electrode (RE), working electrode (WE), and counter electrode (CE). The Open Circuit Potential (OCP), which represents the voltage generated between the working electrode (WE) and reference electrode (RE) in an electrochemical system during cathodic and anodic reactions, provides insights on the behavior of materials in specific electrolytes. The experimental setup involved the utilization of base metal and friction stir welded materials as working electrodes (WEs), with a graphite rod serving as the counter electrode (CE) and a KCl electrode as the reference electrode (RE). The anodic and cathodic potentials were measured to be 1.5 V and −1.5 V, respectively, using a scan rate of 0.005 V/s. The samples of base metals and friction stir welded specimens were immersed in a corrosive solution for a duration of 10 min prior to the measurement of the open circuit potential (OCP). This facilitated the achievement of a stable-state potential and enabled the immediate recording of polarization resistance (PDP) values. The experiment was conducted in triplicate for each corrosion sample, and the mean value was computed and documented. The polarization potential (E_{corr}) and current density (i_{corr}) values were derived from the Tafel curves, which were constructed using the data collected from the linear sweep voltammetry (LSV) data sheet. The calculation of the inhibition efficiency (IE) was performed using equation (1).

$$IE(\%) = \left(1 - \frac{i_{corr}}{i_{ocorr}}\right)100. \quad (1)$$

3 Results and discussion

The weldment generated with the utilization of TT and TTT may be observed in Figure 2a and b. Welding was achievable within the designated range of process variables. However, it was observed that the surface quality varied among the samples, which were subjected to varying factors, in both the TT and TTT weldments.

3.1 Corrosion analysis for parent materials and friction stir welded joints

The extent of corrosion in each environment characterizes the velocity at which the metal transitions towards its equilibrium condition. The amount of this phenomenon is contingent upon various factors, including grain sizes, material composition, and the nature of the corrosive environment. Understanding the corrosion rate is crucial for assessing the anticipated lifespan of the material. The findings indicate that the presence of finer grains promotes an increase in material hardness, which subsequently facilitates the establishment of a passive layer. Consequently, this reduces the likelihood of corrosion. The phenomenon of corrosion leads to gradual and cumulative material deterioration [21,22]. However, it should be noted that the presence of coarse grains frequently promotes the formation of an active coating, leading to an elevation in the rate of corrosion [20]. The corrosion test results are presented in Table 3, which includes data obtained at a rotational speed of 1500 rpm, transverse speeds of 30, 60, and 90 mm/min, and a tool tilt angle of 2 degrees. A comprehensive evaluation of the weldments was conducted in order to examine the impact of various parameters on their corrosion characteristics. Figures 3 and 4 depict the OCP and Tafel plots for both the base metals and the friction stir welded samples, respectively. The corrosion inhibition capability of weldments rises with prolonged exposure time due to the creation of more passive layers, resulting in enhanced corrosion resistance. Yuan et al. [23] have reported that the chemical composition of the passive layer and its ability to effectively hinder corrosion are significantly influenced by the presence of alloying elements, specifically aluminum in this particular instance, as well as the duration of natural passivation.

The weldments denoted as TT_{11} and TTT_{11}, TT_{15} and TTT_{15}, and TT_{12} and TTT_{12} correspond to three different sets of parameters. These parameters include a rotational speed of 1500 rpm, a traverse speed of 30 mm/min, and a tool tilt angle of 2° for the first set; a rotational speed of 1500 rpm, a traverse speed of 60 mm/min, and a tool tilt

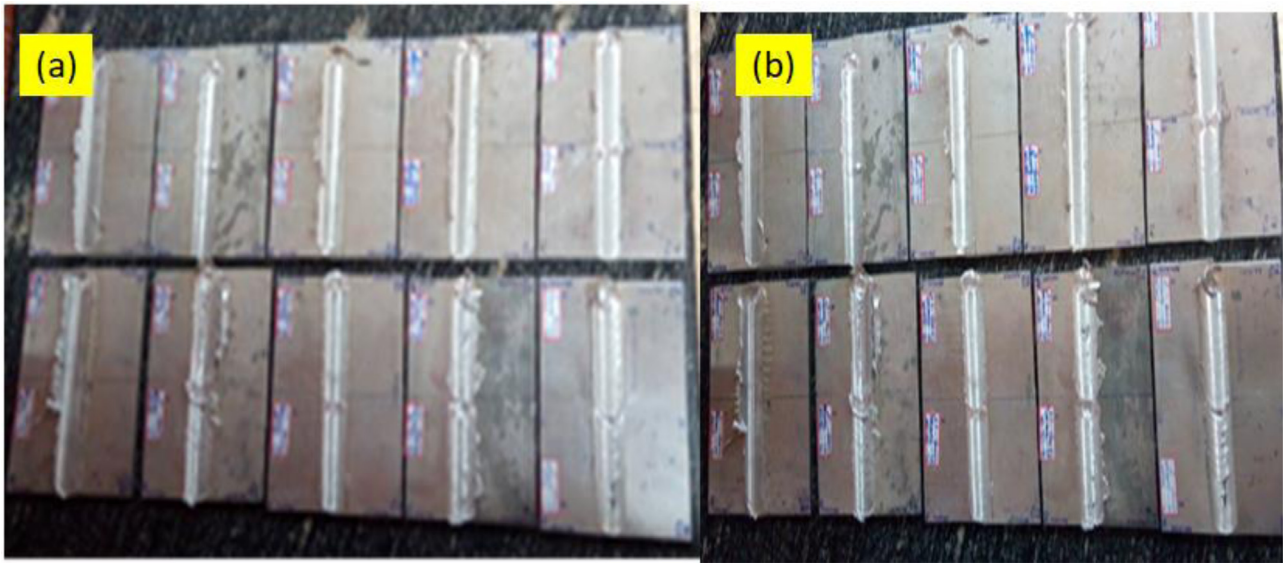

Fig. 2. Weldments (a) Tapered tools (b) Tapered threaded tools.

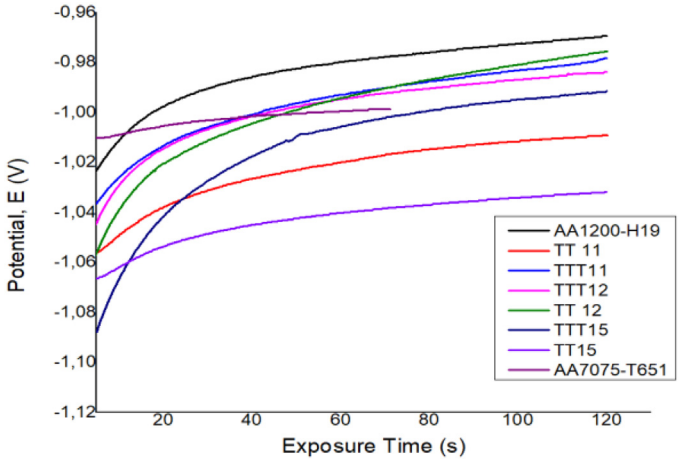

Fig. 3. Open circuit potential against exposure time.

angle of 2° for the second set; and a rotational speed of 1500 rpm, a traverse speed of 90 mm/min, and a tool tilt angle of 2° for the third set.

Based on the findings of the corrosion test, it was seen that the TTT_{11} weldment exhibited the maximum polarization resistance, whereas the base metals AA7075-T651 and AA1200-H19 showed comparatively lower resistance to corrosion. The TTT_{15} compound exhibited the highest percentage inhibitory efficiency, reaching 87.96%. The data presented in the table demonstrates a negative correlation between transverse speed and polarisation resistance. The processing combination of rotational and welding speeds generates uniformly distributed material ripples on the surface of the joints. Specifically, as the transverse speed increases from 30 to 90 mm/min, the polarisation resistance decreases. However, at low rotational speeds, the surface appearance of the joints fabricated by concentric circle shoulder tools is rough and fuzzy as a result of the limited degree of mixing. This position is consistent with the one advanced by Raturi and Bhattacharya [24], who studied friction stir welded dissimilar AA7075-T651 and AA2014-T6 for application in marine and aerospace environments. This relationship is significant as polarisation resistance is directly associated with corrosion rate. The observed parameter exhibited a drop from 478.28 Ω under the TT_{11} condition to 403.14 Ω when the transverse speed was increased from 30 to 60 mm/min (TT_{15}), and then reduced to 223.90 Ω when the transverse speed was further increased to 90 mm/min. The weldments of tapered threaded tools exhibited a similar trend, as illustrated in Table 3. Both TT_{15} and TTT_{15} weldments achieved optimal IE values of 80.12% and 87.96%, respectively. This aligns with the findings of a previous study conducted by Salleh et al. [25], which concluded that an increase in temperature leads to a decrease in IE. Not only are low tool rotation speeds, even at high traverse speeds, unable to sufficiently generate enough heat to cause plastic flow and, hence, adequate diffusion and bonding between the fusing materials, they can also trigger tunnelling defects in the joint, which could be responsible for the trends seen in Table 3. This is because, at such high traverse speed, the tool is unable to absorb enough heat to deliver proper bonding to the joint [24]. Likewise, high tool rotation and markedly low traverse speed result in excess heat, thus causing inadequate material delivery owing to poor friction and material slippage. Therefore, the importance of optimizing process parameters cannot be overemphasized for balanced heat generation, proper bonding and good strength of FSW joints. This conclusion is reported across many studies.

Similarly, the findings from polarization experiments indicate a decrease in corrosion current density, implying that the compounds exhibit effectiveness by adsorption on

Table 3. Corrosion outcome for parent materials and friction stir welded joints.

Samples	Corrosion potential (mV)	% IE	Open circuit potential (v)	Polarization resistance (Ω)	Corrosion rate (mm/yr)	Cathodic Tafel slope (mV/dec)	Corrosion current ($\mu A/cm^2$)	Anodic Tafel Slope (mV/dec)	Chi-Sq. value (χ^2)
AA7075	−1328	–	−0.969	49.52	4.529	53.61	402	156.65	2.79 E-06
AA1200	−1424	53.48	−1.032	69.16	1.624	238.24	187	96.64	6273300
TT_{11}	−1450.2	76.07	−0.995	478.28	0.676	183.77	96.2	114.3	54365
TT_{12}	−1325.1	67.16	−0.984	223.9	0.783	87.53	132	59.14	4.92 E-07
TT_{15}	−1282.3	80.12	−0.976	403.14	0.698	45.37	79.9	88.29	3.13E-07
TTT_{11}	−1321.6	78.06	−1.056	956.17	0.464	53.45	88.2	23.18	1.84 E-08
TTT_{12}	−1293.4	82.73	−1.043	798.78	0.574	23.05	69.4	98.61	4.97 E-07
TTT_{15}	−1282.5	87.96	−0.99884	895.75	0.497	36.51	48.4	36.52	5.42 E-05

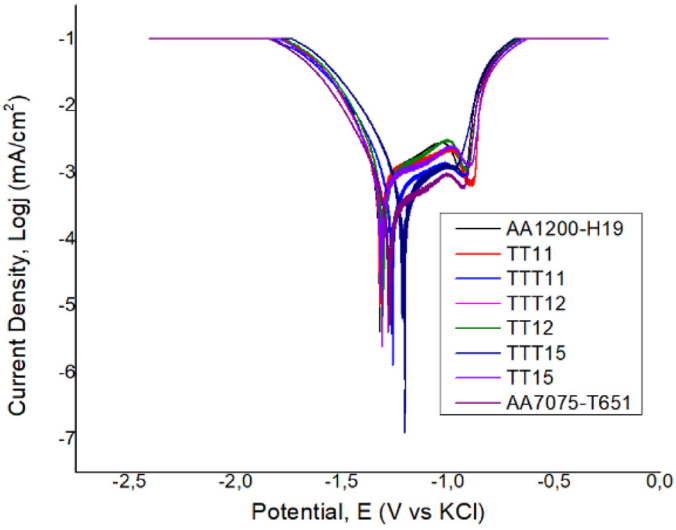

Fig. 4. Tafel diagram for samples of parent metals and friction stir welding.

the active sites of the metal surface [26,27]. It is noteworthy that the anodic and cathodic current densities of the specimens exhibit a high degree of similarity, with TTT_{15} displaying a lower value compared to the other specimens. The spectra obtained using Electrochemical Impedance Spectroscopy (EIS) exhibit distinct characteristics that are both similar and distinctive to the materials employed, featuring additional depressions occurring at a potential below −0.1 V [28]. The underlying cause of this behaviour remains yet to be elucidated in the literature.

The decreasing trend in the corrosion current noticed could also be linked with energy balance concerns often raised about FSW processes. One of the most recent is Ferreira et al. [29], who quantified the effective energy efficiency of FSW processes through the lens of the contributions of processing parameters like tool rotation and traverse speed in order to establish the energy balance of the process. It was revealed that only about $25 \pm 2.9\%$ of the input energy is effectively employed for the welding exercise proper, while a larger part is often dissipated through various components in the experimental set-up.

3.2 Microstructural examination

The microstructure of the weldment obtained using the optimal conditions resulting from the evaluation of the weld integrity was examined with a SEM. Coupons were washed in deionised water, ethanol and dried in hot air prior to observations. The optimal weldment produced with TT and TTT using the optimal conditions was evaluated for the effect of the parameters on their corrosion behaviour. SEM micrographs revealed the extent of corrosion attacks on optimal weldment obtained at 1500 rpm rotational speed, 60 mm/min transverse speed, and a 2° tool tilt angle for both TT and TTT used in evaluating the microstructure and corrosion behaviour of the weldment. The results are presented in Figures 5a-d. Figures 5a and 5b shows that there was sufficient heat to initiate plastic deformation and material coalescence at the optimal welding parameters for both TT and TTT weldments. Also, the corroded weldment for the two optimal samples (Figs. 5c and 5d) indicates that pit attacks and microcracks occurred in its surface topography, which may be as a result of intergranular corrosion on the surface. This is consistent with the report of Barr et al. [30].

The morphology of the corroded coupons of both inhibited and uninhibited metals of both dissimilar AA7075-T651 and AA1200-H19 and their base metals, respectively, was also studied. The morphologies of the extent of corrosion attacks are captured in Figures 5a and 5b. Pit corrosion attacks were predominant in Figures 5a. It is a sign of its vulnerability to corrosion attack; yet, for corroded friction stir welded alloys (the two optimal weldments), intergranular corrosion on the surface caused a significant number of pit attacks as well as microcracks in the surface topography [25]. The ideal and deteriorated weldments of TT15 and TTT15 are shown in Figure 5.

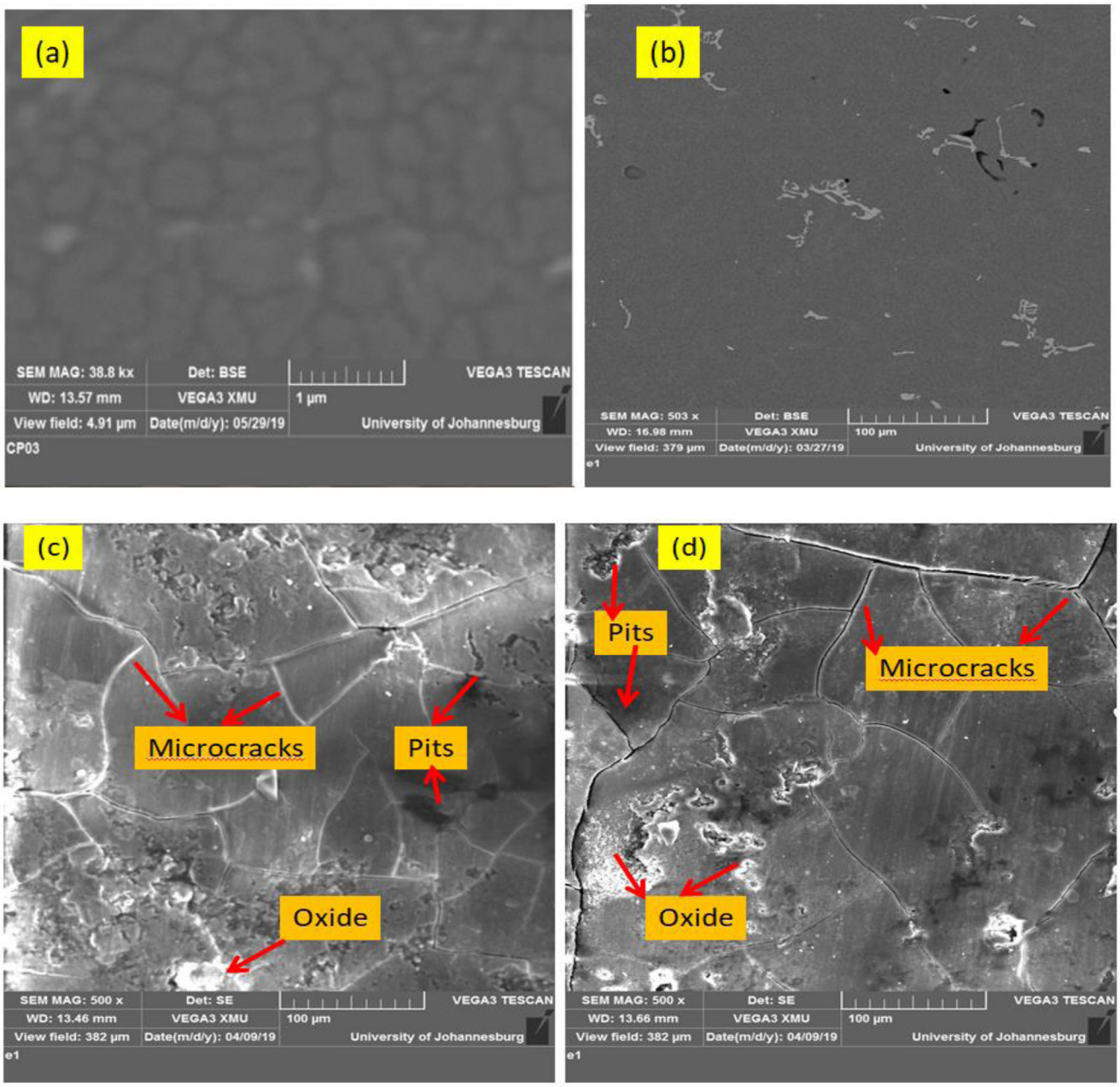

Fig. 5. 500x magnified image for (a) parent metal AA7075 (b) parent metal AA1200 (c) corroded AA7075 alloy (d) corroded AA1200-H19 alloy (e) optimal weldment TT_{15} (f) optimal weldment TTT_{15} (g) corroded optimal TT_{15} (h) corroded optimal TTT_{15}.

3.3 Microstructure of optimized optical welded joints

The rotational motion of the tool at the interface between the tool and the metal facilitates effective blending of the distinct components. The microstructure examination conducted at the weld zone provided insights into the phenomenon of material blending and mass displacement. Figures 6 and 7 demonstrate that under the best welding circumstances for both TT and TTT, an adequate amount of heat was present to facilitate plastic deformation and the fusion of materials. Changes in the weld zones give rise to the formation of three distinct regions. These findings align with the results reported in previous studies [8,31]. The region without mixing is situated in the upper section of the joint, in close proximity to the tool shoulder (as depicted in Figs. 6c and 7c). The mechanically mixed zone is formed by the integration of the microstructures of the alloys AA7075-T651 and AA1200-H19 (see Figs. 6d and 7d). The utilization of Weck's reagent for etching further revealed that the 7075-T651 alloy exhibited a lower weight compared to the AA1200-H19 alloy. The optimal parameters for both tools resulted in a notable degree of material

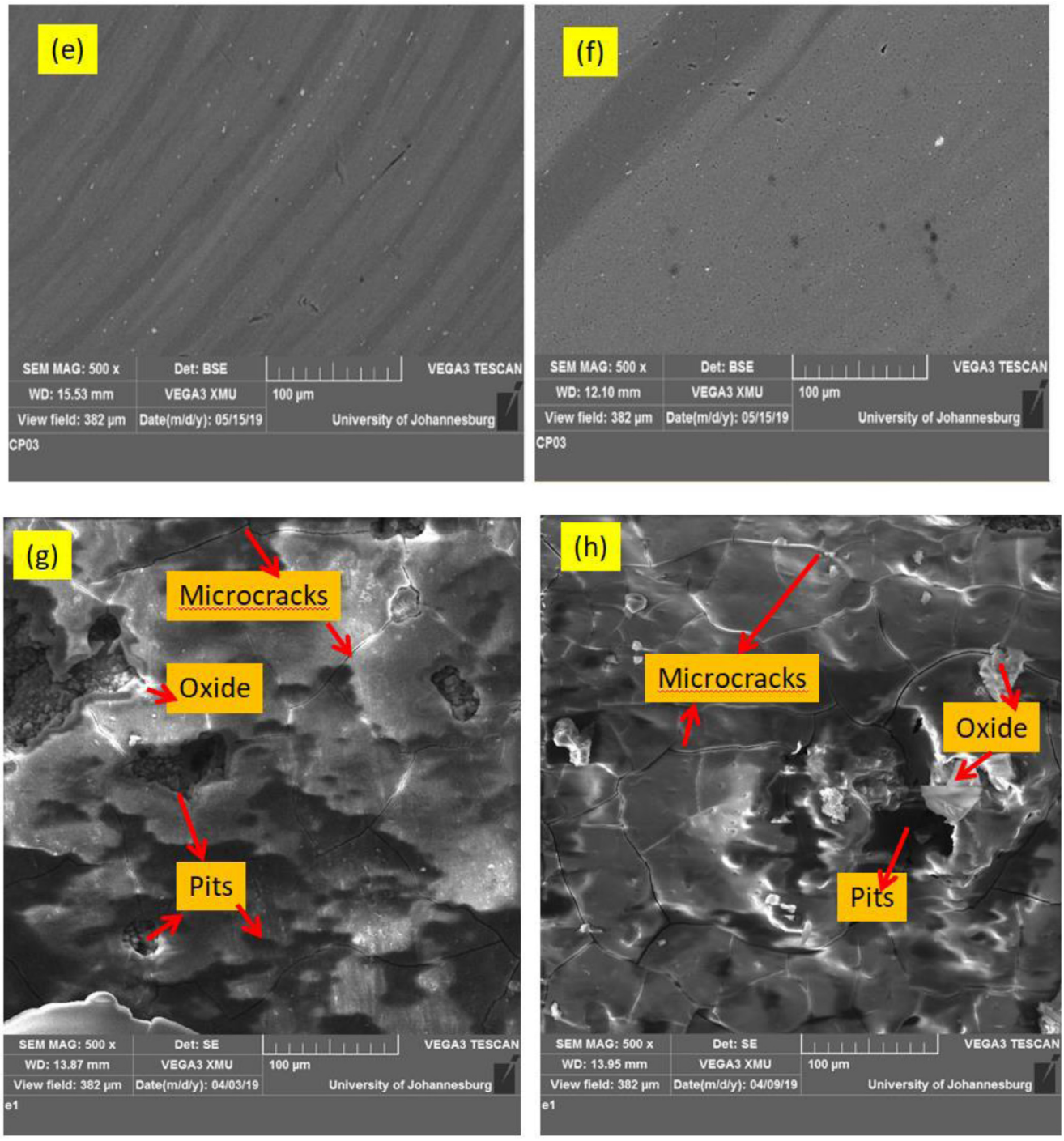

Fig. 5. (Continued).

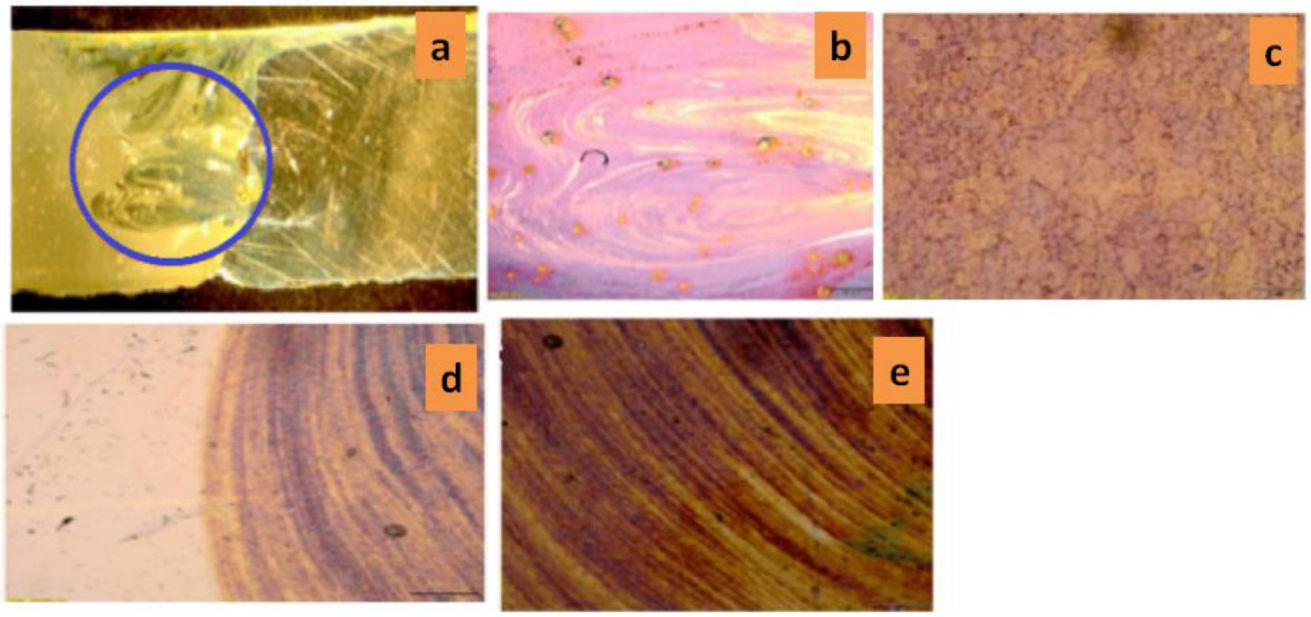

Fig. 6. 100x magnified optical images showing the microstructure and material flow pattern in the nugget zone of the optimal weldment of the tapered tool (a) micrograph of joint, (b) material flow pattern, (c) unmixed, (d) mechanically mixed, (e) mixed region, (blue circle) joint interface.

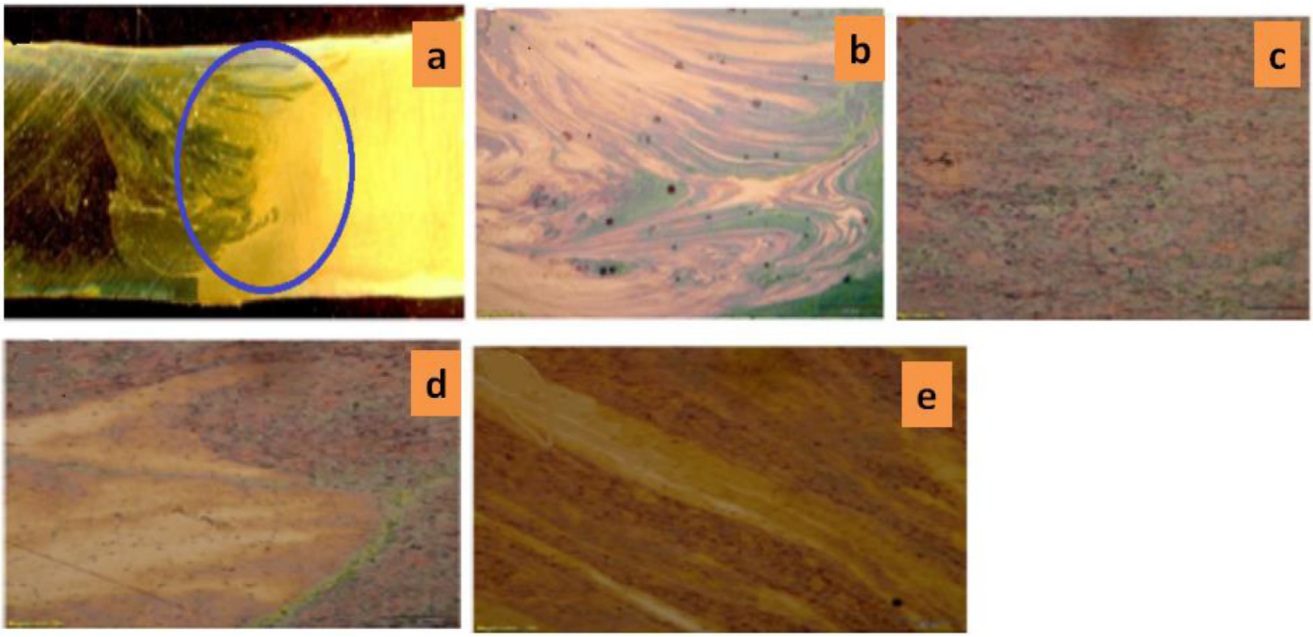

Fig. 7. 100x magnified optical images showing the microstructure and material flow pattern in the nugget zone of the optimal weldment of the tapered threaded tool (a) micrograph of joint, (b) material flow pattern, (c) unmixed, (d) mechanically mixed, (e) mixed region, (blue oval) joint interface.

mixing; hence leading to the formation of onion ring structures in the material flow, as depicted in Figures 6b and 7b. The formation of a mixed zone, which incorporates the microstructure of both alloys, occurs as the materials intermix in alternating layers, as illustrated in Figures 6e and 7e.

4 Conclusions

The successful investigation of the microstructure and corrosion characteristics of dissimilar friction stir welded AA1200-H19 and AA7075-T651 has been conducted for potential industrial applications. Based on the findings acquired, the subsequent deductions can be drawn:

- Irrespective of the tool geometry employed, whether it be TT or TTT, the attainment of a weldment with multiple desired outcomes can be accomplished by employing process parameters such as a rotational speed of 1500 rpm, a welding speed of 60 mm/min, and a tilt angle of 2°.
- The microstructural evolution of the ideal weldments for TT and TTT exhibited similarities, as evidenced by the presence of onion ring formation. This characteristic is indicative of successful alloy mixing during friction stir welding (FSW), resulting in the attainment of exceptional mechanical qualities.
- The anodic or cathodic current densities of the specimens were very close to each other with TTT_{15} lowered than others. The shapes of the Tafel curves differ from the polarisation curves of steel materials with extra small valleys to the left-hand side.
- The rise in transverse speed from 30 to 60 mm/min and subsequently to 90 mm/min resulted in a decrease in polarisation resistance. This observation is consistent with the direct relationship between polarisation resistance and corrosion rate.
- Friction stir welded AA7075-7651 and AA1200-H19 alloys presented an Electrochemical Impedance Spectroscopy (EIS) spectrum which is still to be explored by researchers in this field.

Funding

This research received no external funding.

Conflict of interest

The authors declare no competing interest.

Data availability

Data are available within this article.

Author contribution

B.I. Attah: Conceptualization, methodology, writing-original draft, investigation. R.O. Medupin : Investigation, writing-review & editing. T.D. Ipilakyaa: Validation and investigation, U.G. Okoro: Data Curation and Resources, O. Adedipe: Visualization and Project administration, G. Sule: Methodology and Formal analysis, OM Ikumapayi: software, Investigation, writing-review & editing, TC Jen: software, conceptualization, supervision, funding acquisition. K.C. Bala: Validation, project administration. ET Akinlabi: conceptualization, supervision, funding acquisition. S.A. Lawal: Validation and investigation, A.S. Abdulrahman: Resources and Formal analysis

References

1. L. Li, M. Chakik, R. Prakash, A review of corrosion in aircraft structures and graphene-based sensors for advanced corrosion monitoring, Sensors, **21** (2021). https://doi.org/10.3390/s21092908
2. O.M. Ikumapayi, E.T. Akinlabi, J.D. Majumdar, Review on thermal, thermo-mechanical and thermal stress distribution during friction stir welding, Int. J. Mech. Eng. Technol. **9** (2018) 534–548.
3. D. Mulaba-Kapinga, K.D. Nyembwe, O.M. Ikumapayi, E.T. Akinlabi, Mechanical, electrochemical and structural characteristics of friction stir spot welds of aluminium alloy 6063, Manuf. Rev. **7** (2020) 1–15.
4. R.M. Leal, A. Loureiro, D.M. Rodrigues, I. Galvao, Material flow in heterogeneous friction stir welding of aluminium and copper thin sheets, Sci. Technol. Weld. Join. **5** (2010) 654–660.
5. D.G. Mohan, C. Wu, A review on friction stir welding of steels, Chin. J. Mech. Eng. (2021), https://doi.org/10.1186/s10033-021-00655-3
6. V.P. Singh, S.K. Patel, A. Ranjan, B. Kariachen, Recent research progress in solid state friction-stir welding of aluminium-magnesium alloys: a critical review, J. Mater. Res. Technol. **9** (2020) 6217–6256.
7. D.A. Caio-Palumbo, C. Isolda, G.D. Harcilio, P. Nadine, T. Bernard, V. Vincent, Multiscale electrochemical study of welded aluminium joined by friction stir welding, J. Electrochem. Soc. **164** (2017) 735–746.
8. Y. Wang, H. Jiang, X. Wu, Q. Meng, Microstructure and mechanical property evolution of robotic friction stir-welded Al–Li alloys, Crystals **13** (2023) 582.
9. N.D.T. Pankaj, K.P. Pranav, Optimization of Friction stir welding parameters in joining dissimilar aluminium alloys using SPSS and Taguchi, J. Basic Appl. Eng. Res. **1** (2014) 25–27.
10. E. Fereiduni, M. Movahedi, A.H. Kokabi, Aluminum/steel joints made by an alternative friction stir spot welding process, J. Mater. Process. Technol. **224** (2015) 1–10.
11. M.V. Sezhian, K. Giridharan, D.P. Pushpanathan, G. Chakravarthi, B. Stalin, A. Karthick, P.M. Kumar, M. Bharani, Microstructural and mechanical behaviors of friction stir welded dissimilar AA6082-AA7075 joints, Adv. Mater. Sci. Eng. **2021** (2021) 4113895.
12. T. Yoo, J. Yoon, K. Min, H. Lee, Effect of friction stir welding process parameters on mechanical properties and macro structure of Al-Li alloy, 2nd International Materials, Industrial, and Manufacturing Engineering Conference, February 4th -6th, Bali Indonesia, 2015. Retrieved on November 12 2017 from. http://www.sciencedirect.com.
13. T.J. Lienert, W.L. Stellwag, J.B.B. Grimmett, R.W. Warke, Friction stir welding studies on mild steel, American welding society, Suppl. Weld. J. **35** (2013) 210–224.
14. M.M. Hadi, M.M.H. Al-khafaji, A.D. Subhi, A numerical study of friction stir welding for AA5754 sheets to evaluate temperature profile and plastic strain, Eng. Technol. J. **40** (2022) 1683–1694.
15. K.D. Bhatt, B. Pillai, Simulation of peak temperature and flow stresses during friction-stir welding of AA7050-T7451 aluminium alloy using hyper works, Int. J. Emerg. Technol. Adv. Eng. **2** (2012) 212–216.
16. S. Jambulingam, Optimization of process parameters of friction stir welding for dissimilar aluminium alloys AA7075 and AA3014, Int. J. Emerg. Res. Eng. Sci. Technol. **2** (2015) 234–251.
17. G. Amit, K.R. Punit, K.K. Atul, Optimization of friction-stir welding parameters for AA3003 aluminum alloy joints using response surface methodology, Int. J. Mech. Solids **12** (2017) 15–26.

18. E.T. Akinlabi, E. Annelize, J.M. Patrick, Effect of travel speed on joint properties of dissimilar metal friction-stir welds, Second International Conference on Advances in Engineering and Technology, 20th -21st December, 2012, Noida, India, pp. 155–161.
19. B.I. Attah, S.A. Lawal, K.C. Bala, O.M. Ikumapayi, O. Adedipe, R. P. Mahto, E.T. Akinlabi, Optimization and numerical analysis of friction stir welding parameters of AA7075-T651 and AA 1200-H19 using tapered tool, Int. J. Interact. Des. Manuf. (IJIDeM) (2023), https://doi.org/10.1007/s12008-023-01329-1.
20. O.M. Ikumapayi, E.T. Akinlabi, J.D. Majumdar, O.S.I. Fayomi, S. A. Akinlabi, Corrosion study and quantitative measurement of crystallite size of high strength Aluminum hybrid composite developed via friction stir processing, Materialwiss. Werkstofftech. **51** (2020) 732–739.
21. F. Zhang, J. Pan, Recent development of corrosion protection strategy based on mussel adhesive protein, Front. Mater. **6** (2019). https://doi.org/10.3389/fmats.2019.00207.
22. B.X. Vuong, T.L. Huynh, T.Q.N. Tran, S.V.P. Vattikuti, T.D. Manh, P. Nguyen-Tri, A.T. Nguyen, P. Van Hien, N. Nguyen Dang, Corrosion inhibition of carbon steel in hydrochloric acid solution by self-formation of a Malpighia glabra leaf extract-based organic film, Mater. Today Commun. **31** (2022) 103641.
23. X. Yuan, X. Wang, Y. Cao, H. Yang, Natural passivation behaviour and its influence on chloride-induced corrosion resistance of stainless steel in simulated concrete pore solution, J. Mater. Res. Technol. **9** (2020) 12378–12390.
24. M. Raturi, A. Bhattacharya, Mechanical strength and corrosion behavior of dissimilar friction stir welded AA7075-AA2014 joints, Mater. Chem. Phys. **262** (2021) 124338.
25. S.Z. Salleh, A.H. Yusoff, S.K. Zakaria, M.A.A. Taib, A. Abu Seman, M.N. Masri, M. Mohamad, S. Mamat, S. Ahmad Sobri, A. Ali, P. Ter. Teo, Plant extracts as green corrosion inhibitor for ferrous metal alloys: a review, J. Clean. Prod. **304** (2021).
26. O.M. Ikumapayi, E.T. Akinlabi, Recent advances in keyhole defect repairs via refilling friction stir spot welding, Mater. Today: Proc. **18** (2019) 2201–2208.
27. R.O. Medupin, K. Ukoba, K.O. Yoro, T.-C. Jen, Sustainable approach for corrosion control in mild steel using plant-based inhibitors: a review, Mater. Today Sustain. **22** (2023) 100373.
28. Y. Wang, J. Hu, Y. Ma, Z. Zhang, H. Huang, J. Wei, S. Yin, Q. Yu, A novel high-efficient MOFs-based corrosion inhibitor for the reinforcing steel in cement extract, Constr. Build. Mater. **317** (2022) 125946.
29. F.B. Ferreira, P. Vilaça, J.P. Oliveira, T.G. Santos, P.L. In, Assessment of the energetic efficiency of friction stir welding /processing. **103** (2023) 298–308.
30. C.M. Barr, S. Thomas, J.L. Hart, W. Harlow, E. Anber, M.L. Taheri, Tracking the evolution of intergranular corrosion through twin-related domains in grain boundary networks, Npj Mater. Degrad. August 2017, (2018) 1–10.
31. O.M. Ikumapayi, E.T. Akinlabi, J.D. Majumdar, S.A. Akinlabi, Characterization of high strength aluminium – based surface matrix composite reinforced with low-cost PKSA fabricated by friction stir processing, Mater. Res. Express. **6** (2019) 1–27.

Cite this article as: Benjamin I. Attah, RASAQ O. Medupin, Tertsegha D. Ipilakyaa, Uzoma G Okoro, Oyewole Adedipe, Gowon Sule, Omolayo Michael Ikumapayi, Katsina C. Bala, Esther T. Akinlabi, Sunday A. Lawal, Asipita S. Abdulrahman Microstructural and corrosion behaviours of dissimilar friction stir welded aluminium alloys, Manufacturing Rev. **11,** 7 (2024)